JOURNAL OF MATERIALS SCIENCE **33** (1998) 5205–5220

Eutectic solidification characteristics of Bridgman grown Al-3Fe-0.1V alloy

Y. WANG, H. JONES
Department of Engineering Materials, University of Sheffield, Mappin Street, Sheffield, S1 3JD, UK

P. V. EVANS
Alcan International Limited, Banbury Laboratory, Southam Road, Banbury, Oxon, OX16 7SP, UK

Eutectic solidification characteristics of Al-2.85 wt %Fe-0.12 wt %V alloy have been investigated by steady-state growth over the range of solidification front velocity from 51 to 1030 μm/s and temperature gradient 8 to 15 K/mm. Increasing growth velocity displaced the αAl-Al_3Fe eutectic by αAl-Al_xFe eutectic rather than by the αAl-Al_6Fe eutectic obtained for the binary Al-3 wt %Fe alloy. A fully αAl-Al_xFe eutectic structure has been obtained for the first time in the vanadium-containing alloy over the growth velocity range from 71 to 1030 μm/s except at 100 and 510 μm/s where some αAl dendrites were present in the eutectic matrix. The αAl-Al_xFe eutectic was observed to undergo a morphological transition from lamellar to rod-like with increasing growth velocity concurrently with formation of a cellular eutectic structure. It was found that the relationship $\lambda = Av^{-1/2}$, between eutectic spacing λ and growth velocity v, was applicable with $A = 22.4 \pm 1.8$ and 13.8 ± 2.1 $\mu m^{3/2} s^{-1/2}$ for lamellar and rod-like αAl-Al_xFe eutectics, respectively.

1. Introduction

Pioneering work [1–3] on steady state Bridgman growth of Al-rich Al-Fe alloys established the solidification characteristics of two competing eutectics, stable αAl-Al_3Fe and metastable αAl-Al_6Fe. It was shown that αAl-Al_3Fe eutectic is replaced by αAl-Al_6Fe eutectic at sufficiently high growth velocity. Fully αAl-Al_6Fe eutectic structure was obtained in hypereutectic binary Al-Fe alloys over a limited range of iron concentration by controlling solidification conditions during steady-state growth [1, 3]. Some other metastable binary intermetallic phases, Al_mFe ($m = 4$–4.4) [4], Al_xFe ($x = 5$–5.8) [5–7], Al_pFe ($p = 4$) [8] and Al_9Fe_2 [9], have also been observed in the alloy system.

Several authors have studied the influences of further additions, including Cu, Mg, Mn, Zn, Si, Ti, Co and Ni, on solidification microstructures and eutectic characteristics of Al-Fe alloys [10–13]. It has been shown that such further additions, even in small amounts, can result in significant changes in the relative stability of these intermetallic phases so that the solidification microstructures formed as a result of competition between these phases were considerably affected. Different structure for the eutectics also resulted from the presence of the additions. The present study was to examine the influence of 0.1 wt % vanadium on the eutectic solidification characteristics of Al-3 wt %Fe alloy.

2. Experimental

Al-3 wt %Fe base alloys were provided by Alcan International Ltd, Banbury Laboratory based on high purity 99.99% aluminium and an Al-5.2 wt %Fe master alloy and supplied as 10 mm diameter rods. The actual compositions of the alloys are given in Table I. Received alloy rods were subsequently swaged and drawn to 2.8 mm in diameter. Samples 110 mm long were unidirectionally solidified using 3 mm bore and 4 mm outside diameter alumina tube as a crucible in a vertical Bridgman apparatus at growth velocities between 51 and 1030 μm/s with an imposed temperature gradient of 8 to 15 K/mm.

The alloy samples which had been unidirectionally solidified were examined by optical and electron microscopy as well as by X-ray diffractometry (XRD). Both transverse and longitudinal sections of the samples were polished followed by etching in Keller's reagent and then examined by standard optical metallography. To reveal the solidified eutectic morphology in three dimensions, some of the samples were further deeply etched in 10 vol % hydrochloric acid aqueous solution at room temperature to remove the αAl matrix. Scanning electron microscopy (SEM) observations on the deep etched surfaces of the samples were performed by using a JEOL6400 scanning electron microscope. 3 mm diameter discs were made by slicing the samples

TABLE I Alloy compositions for Bridgman growth (wt %)

Nominal composition	Fe	V	Cu	Mg	Si	Al
Al-3.0Fe	3.00	*	*	*	*	Bal.
Al-3.0Fe-0.1V	2.85	0.12	*	*	*	Bal.

*indicates < 0.01 wt %

transversely followed by hand grinding to a thickness of about 100 microns. Thin foils for transmission electron microscopy (TEM) observations were produced from these by standard electropolishing in a methanol solution containing 25 vol % nitric acid at about −25 °C. TEM was carried out in a Philips EM400T microscope. XRD was performed using a Philips 1700 X-ray diffractometer with CoK_α radiation. Samples for XRD were in the form of powder which was obtained by filing the samples. The phases were identified by combining TEM selected area electron diffraction and XRD with reference to XRD patterns given in the JCPDS files in the case of well verified equilibrium phases, and to those found in the literature in the case of non-equilibrium and less well defined structures.

3. Results

3.1. Solidification microstructure

Table II presents the solidification microstructure and eutectic morphology as function of solidification front velocity for the Al-2.85Fe-0.12V alloys, compared to the binary Al-3Fe alloy. It is seen that addition of 0.12 wt % vanadium to the binary alloy significantly promoted the formation of αAl-Al_xFe eutectic in the growth velocity range of the present study. With increasing growth velocity, αAl-Al_3Fe (Eu1) was displaced by metastable αAl-Al_xFe (Eu3) rather than by the αAl-Al_6Fe eutectic (Eu2) found in the binary alloy. The eutectic transition was, in both cases, accompanied by an elimination of primary Al_3Fe intermetallic phase. In the present study, a fully αAl-Al_xFe eutectic structure was obtained in the vanadium-containing alloy over the growth velocity range from 71 to 1030 μm/s except at 100 and 510 μm/s where a low volume fraction of primary αAl dendrites was present in the Eu3 eutectic matrix.

3.2. Eutectic morphology

Table II gives a brief description of the morphology of eutectics αAl-Al_3Fe (Eu1), αAl-Al_6Fe (Eu2) and αAl-Al_xFe (Eu3) formed at different velocities in the two alloys. Eu1 present in both alloys was plate-like with no obvious difference in morphology attributable to added vanadium. Fig. 1 shows Eu1 with some primary Al_3Fe in the Al-2.85Fe-0.12V alloy grown at 51 μm/s. Eu2 formed in the binary alloy from 91 to 1030 μm/s was rod-like. A cellular Eu2 eutectic structure, as reported by Hughes and Jones [3], was observed to have developed for the binary alloy at 200 μm/s and higher velocities.

Fig. 2a to d show the typical morphology of Eu3 present in the vanadium-containing alloy Bridgman

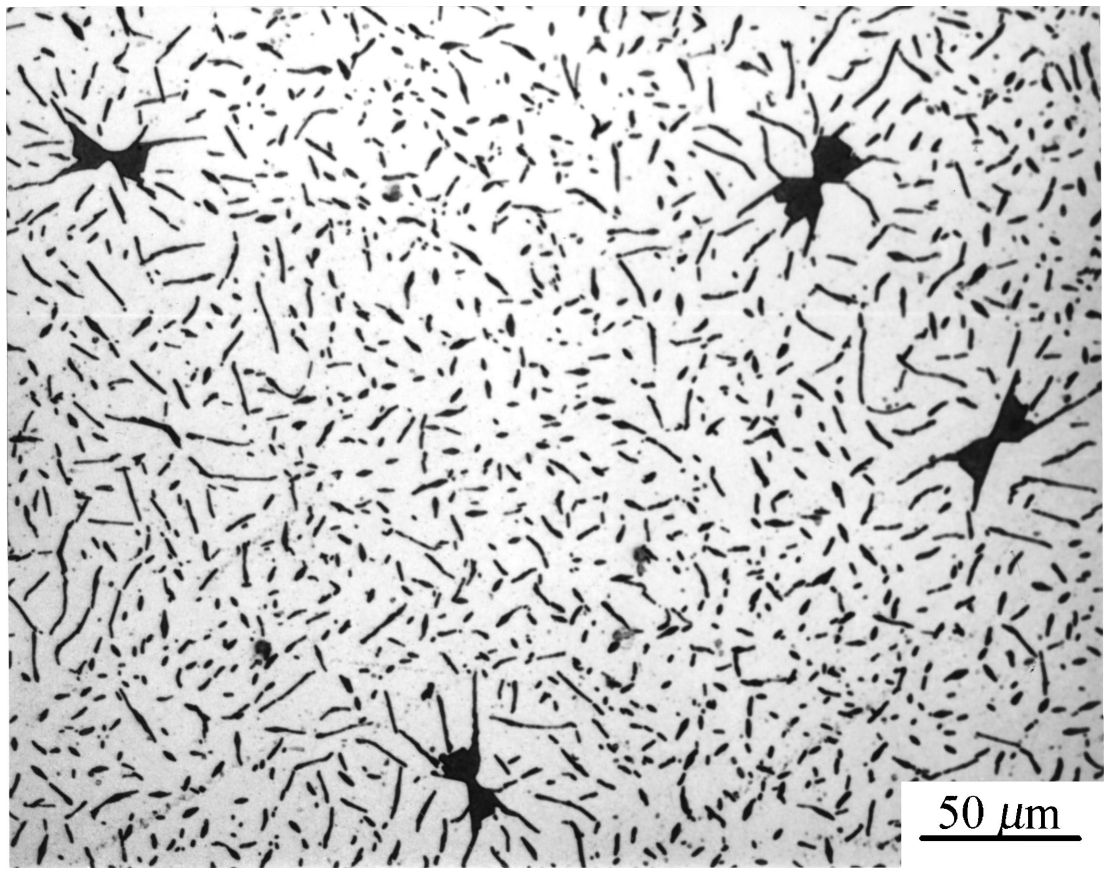

Figure 1 Optical micrograph showing plate-like αAl-Al_3Fe eutectic plus primary Al_3Fe intermetallic crystals in Al-2.85Fe-0.12V alloy grown at 51 μm/s.

TABLE II Solidification microstructure and eutectic morphology for Al-3Fe and Al-2.85Fe-0.12V alloys as a function of growth velocity

Growth velocity (μm/s)	Solidification microstructure		Morphology of eutectic	
	Al-3.0Fe	Al-2.85Fe-0.12V	Al-3.0Fe	Al-2.85Fe-0.12V
1030	Eu2	Eu3	R, C	R, C
810	Eu2	Eu3	R, C	R, C
510	Eu2	(α) + Eu3	R, C	R + BL + L
340	Eu2	Eu3	R, C	L + BL + R
200	Eu2	Eu3	R, C	L + BL + R
100		(α) + Eu3		L + BL
91	Eu2	Eu3	R	L + BL
81		Eu3		L + BL
71	$\beta + \alpha$ + Eul	Eu3	P	L + BL
60		$\beta + \alpha$ + Eul		P
51	$\beta + \alpha$ + Eul	$\beta + \alpha$ + Eul	P	P

α = dendritic αAl solid solution, β = primary Al_3Fe, Eu1 = αAl-Al_3Fe eutectic, Eu2 = αAl-Al_6Fe eutectic, Eu3 = αAl-Al_xFe eutectic, P = plate-like, L = lamellar, BL = broken lamellar, R = rod-like, C = cellular.

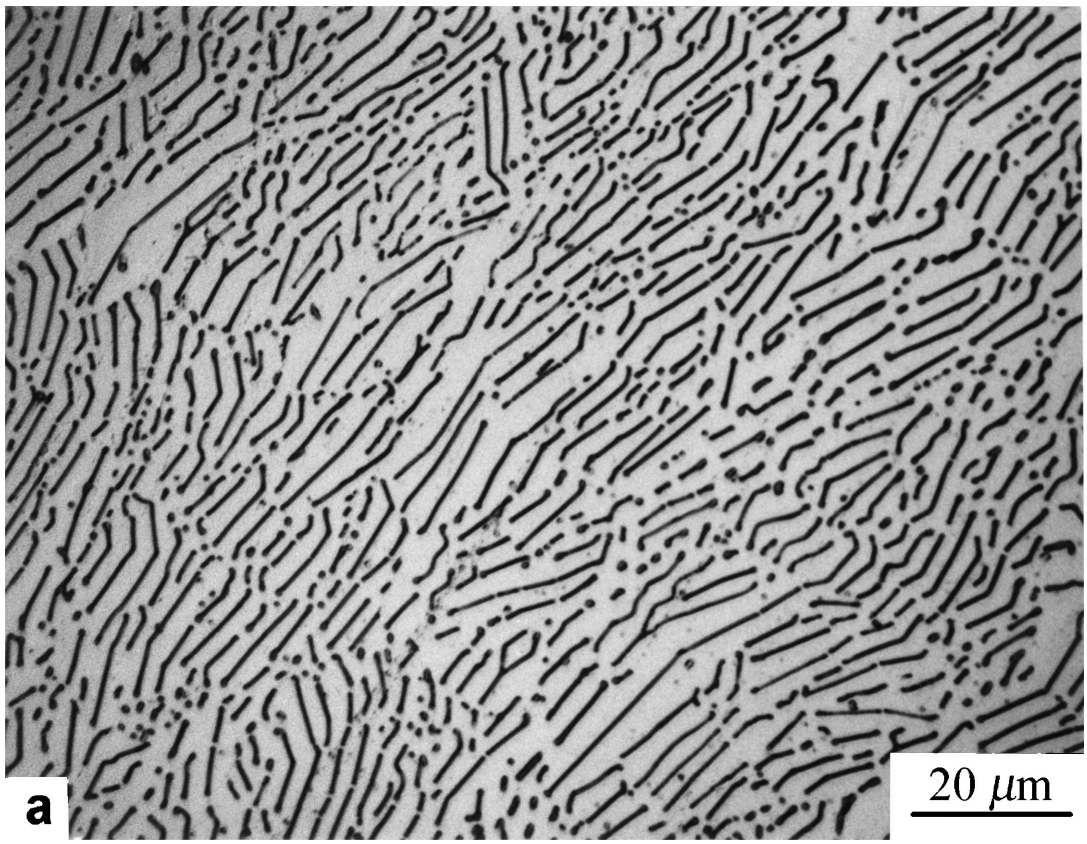

Figure 2 Typical lamellar αAl-Al_xFe eutectic in Al-2.85Fe-0.12V grown at (a) 91, (b) 200, (c) 200 (longitudinal), (d) 340 μm/s and (e) [100] selected area electron diffraction pattern of Al_xFe. (*Continued*).

grown at 91, 200 and 340 μm/s and Fig. 2e is a [100] selected electron diffraction pattern of the eutectic, which indicates that its second phase is metastable Al_xFe intermetallic with the monoclinic crystal structure suggested by Young and Cline [5]. Fig. 2a to d show that Eu3 formed at these growth velocities is essentially lamellar even though limited rod-like morphology is displayed in a few localised regions. Some of the lamellae were found to be segmented even at velocity as low as 71 μm/s and the tendency to segment increased with increasing growth velocity so that the rod-like morphology was dominant in the sample grown at 510 μm/s, as shown in Figs 3a, b, in which only a few lamellae with small aspect ratio remain. The Al_xFe eutectic lamellae were aligned only locally and not always perfectly parallel to each other. Zigzagged and curved lamellae were occasionally observed, as shown in Figs 2a to d and Fig. 4. Primary αAl dendrites present in the Eu3 matrix of Al-2.85Fe-0.12V grown at 100 μm/s were suppressed at higher velocities but re-appeared at 510 μm/s, as shown in Fig. 3a. These primary αAl dendrites were found to be surrounded by Al_xFe lamellae which tended to exhibit a dog-bone morphology in section (Figs 3b, 4 and 5). There was no pronounced difference in Eu3 morphology because of the presence of this primary αAl phase.

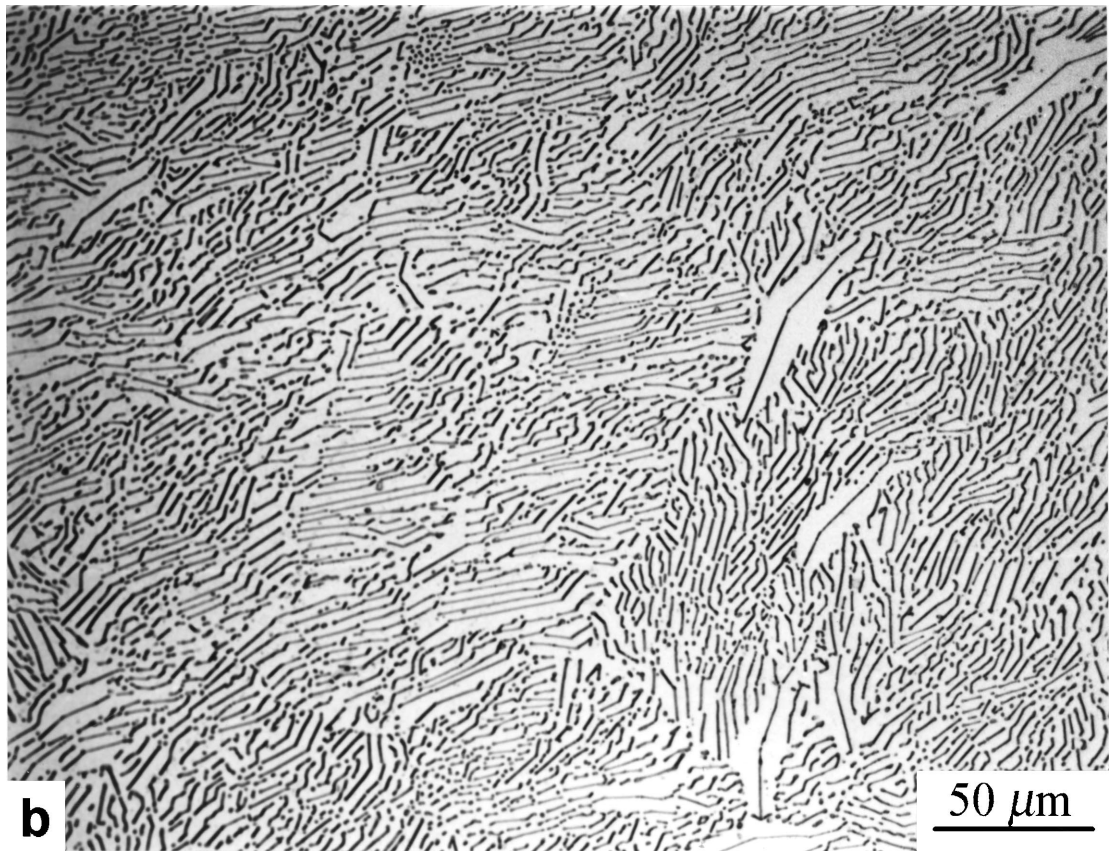

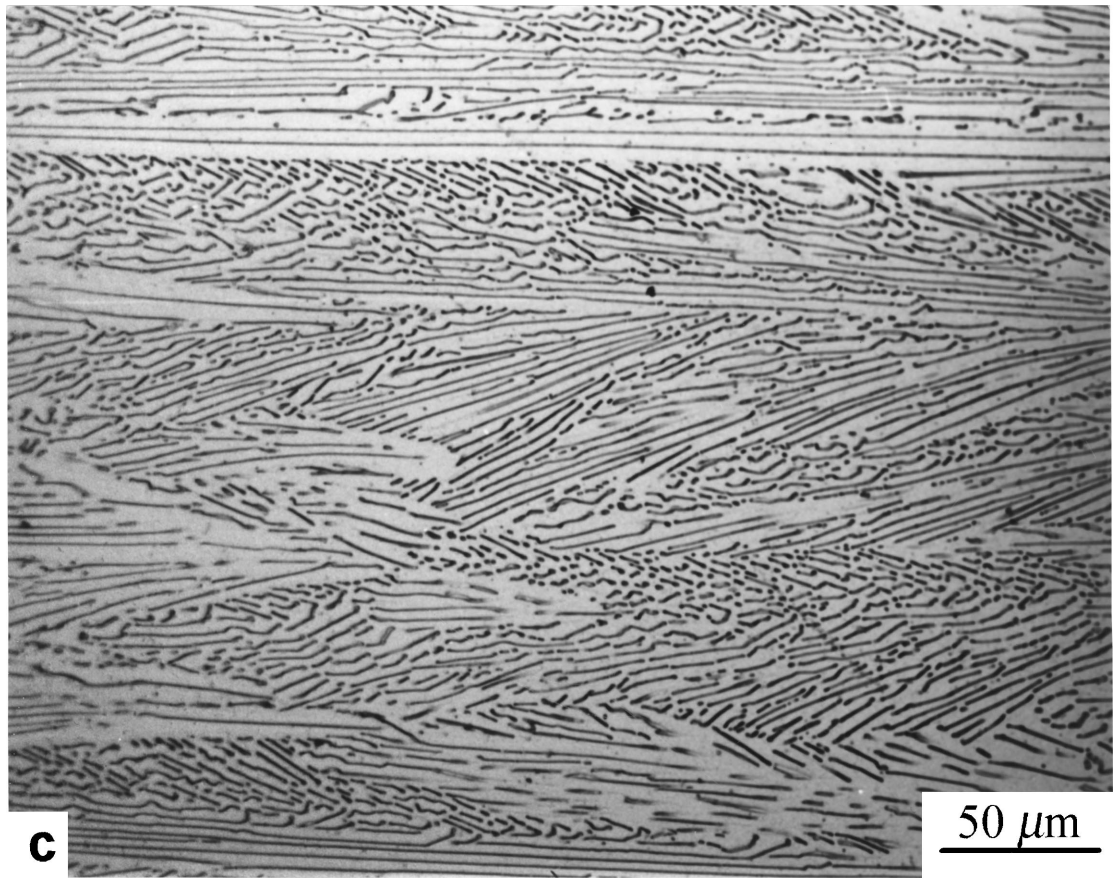

Figure 2 (*Continued*).

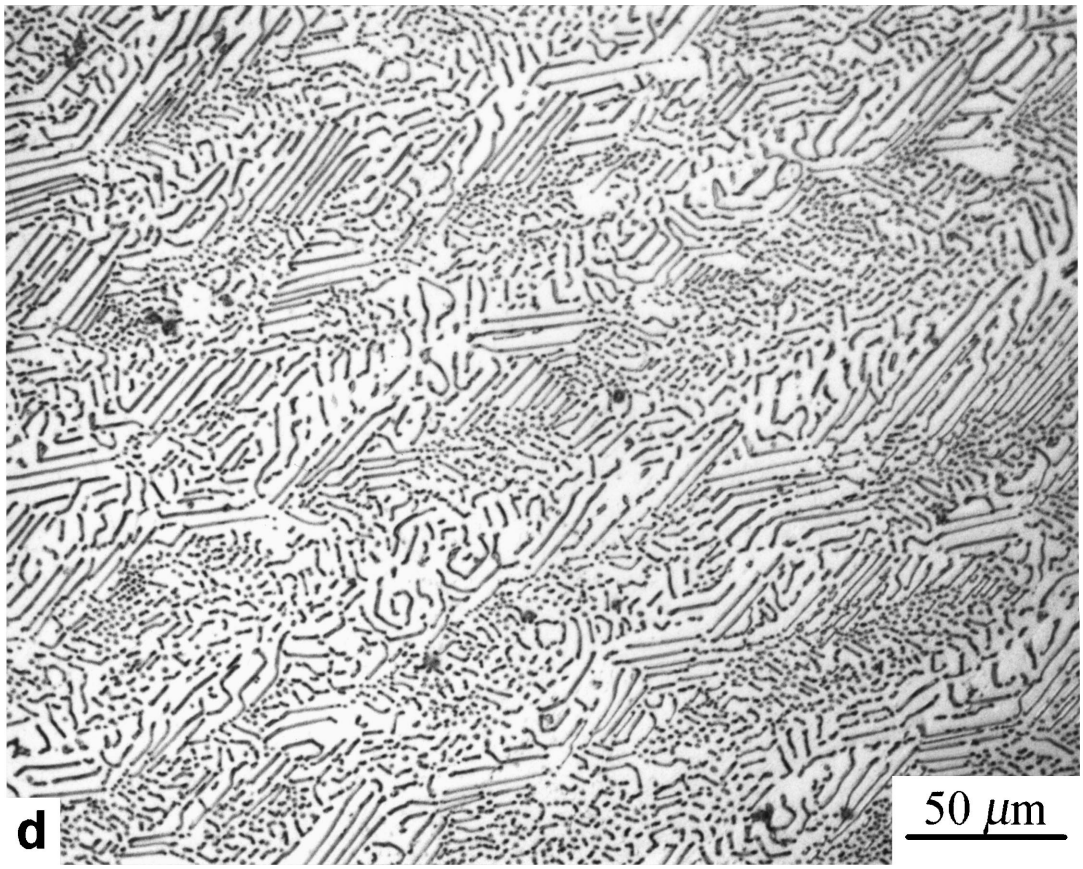

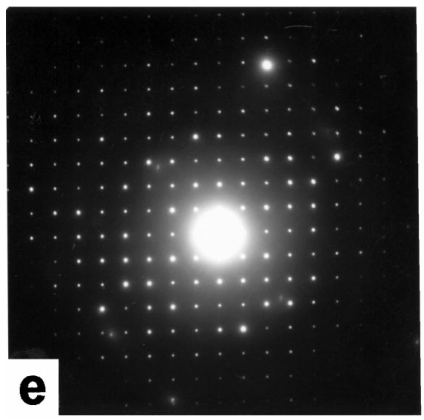

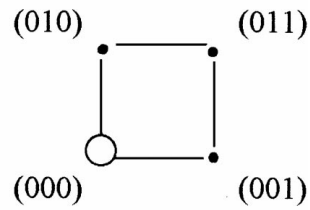

Figure 2 (*Continued*).

SEM observations on deeply etched samples which showed a coexistence of lamellar and rod-like morphologies of Eu3 revealed the evidence of breaking-up of the lamellae with linking of the rods. Figs 6a to d show the typical 3-dimensional growth morphologies of Al_xFe in Eu3 observed along both transverse and longitudinal directions in the samples grown at 200 and 340 μm/s. A lateral branching of Al_xFe lamellae, shown in Fig. 6b, is particularly notable. This was observed also in a dilute Al-Fe-Si alloy by Todd and Jones [11] who found that the skeletal Al_xFe crystal showed no difference in orientation between the main body and the protrusions except for a small deviation which was attributed to crystal curvature. This lateral branching of the lamellae explains why apparently rod-like Al_xFe was evident in polished longitudinal surfaces, as shown in Fig. 2c. As shown in Figs 6c and d, both lamellae and rods appeared in a single eutectic grain and the segmentation of lamellae is evident. Branching of rods and lamellae was seen, as shown in Figs 7a and b, in local areas of the sample grown at 510 μm/s. Those lamellae with small aspect ratio seen in Figs 3a, b and 5 were considered to have resulted from sectioning through rods near to their point of branching and through lamellae which were close to being segmented.

The eutectic Al_xFe lamellae formed at low growth velocities usually displayed a zigzagged and curved morphology in transverse section. Those with small aspect ratio showed a dog-bone section morphology which was similar to the findings of Young and Clyne [5] and Todd [15]. The lamellar eutectic structure became less stable with increasing growth velocity and

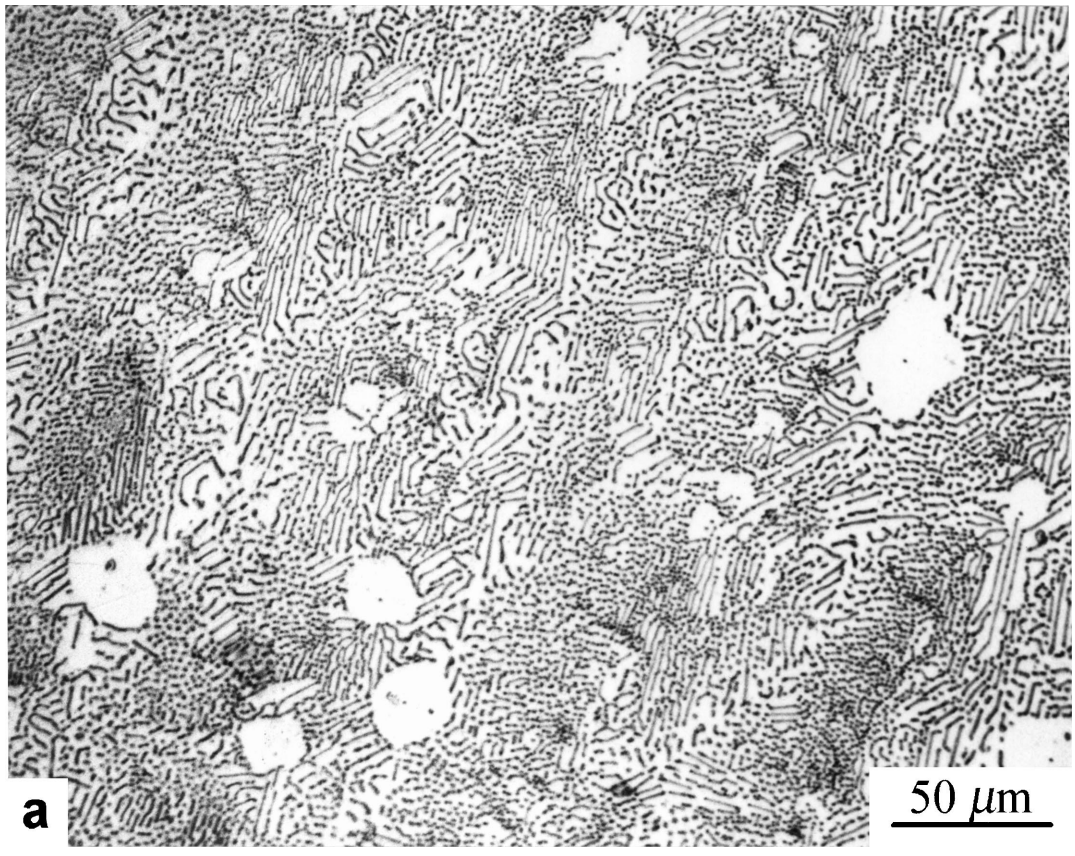

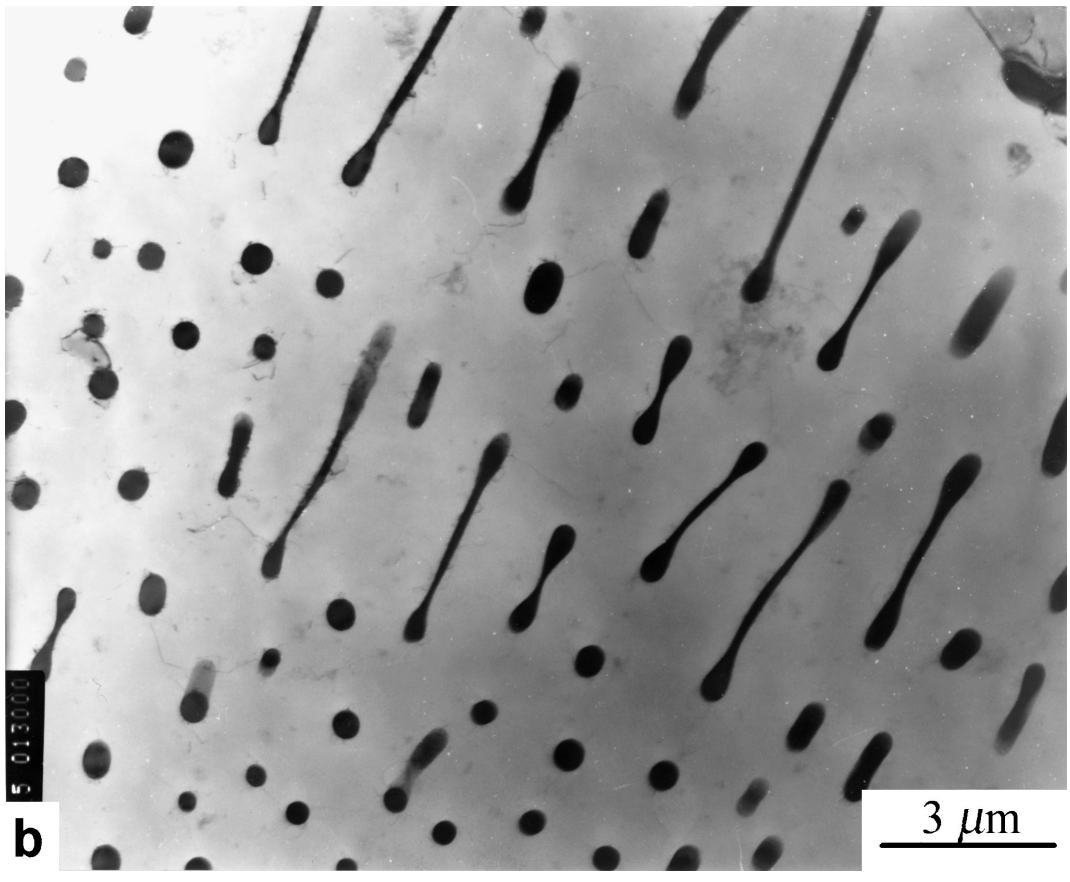

Figure 3 Optical and TEM micrographs showing coexistence of lamellar and rod-like αAl-Al$_x$Fe eutectic in Al-2.85Fe-0.12V alloy grown at 510 μm/s.

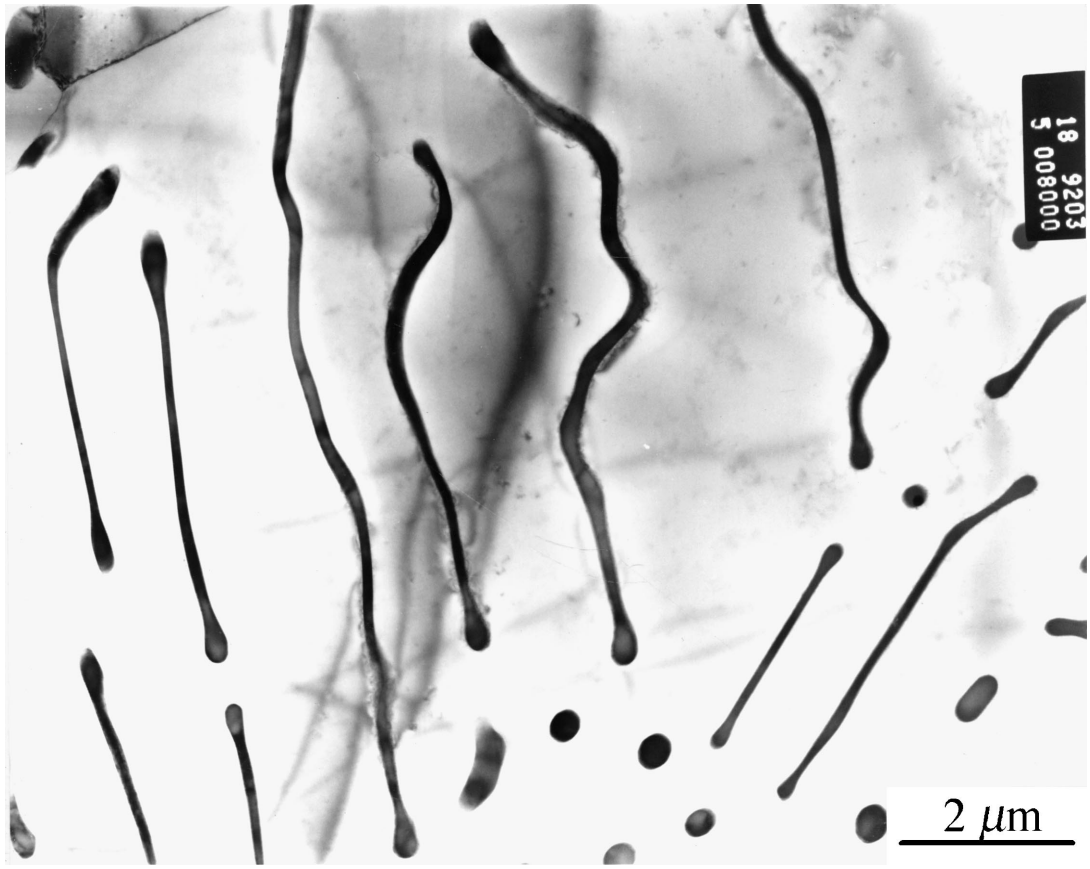

Figure 4 TEM micrograph showing curved Al_xFe eutectic lamellae in Al-2.85Fe-0.12V alloy grown at 200 μm/s.

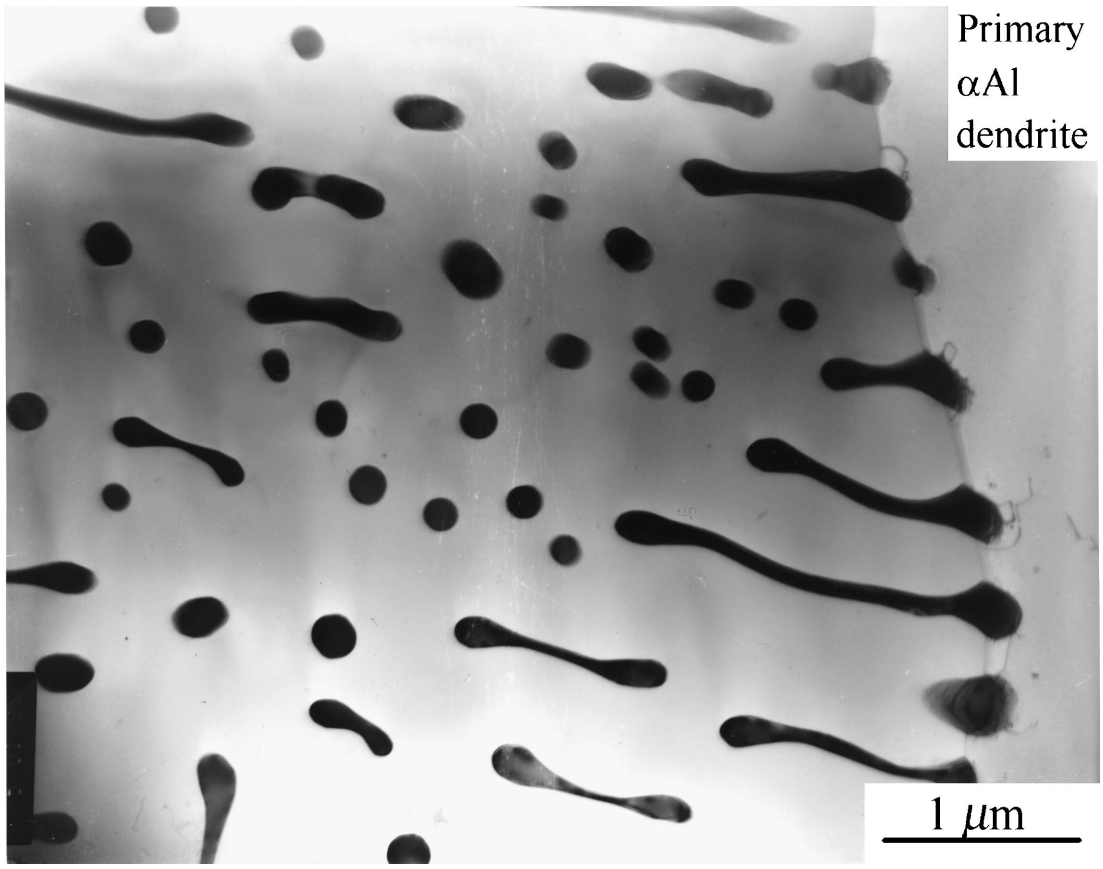

Figure 5 TEM micrograph showing dog-bone sectioned morphology of Al_xFe eutectic lamellae surrounding primary αAl dendrites in Al-2.85Fe-0.12V alloy grown at 510 μm/s.

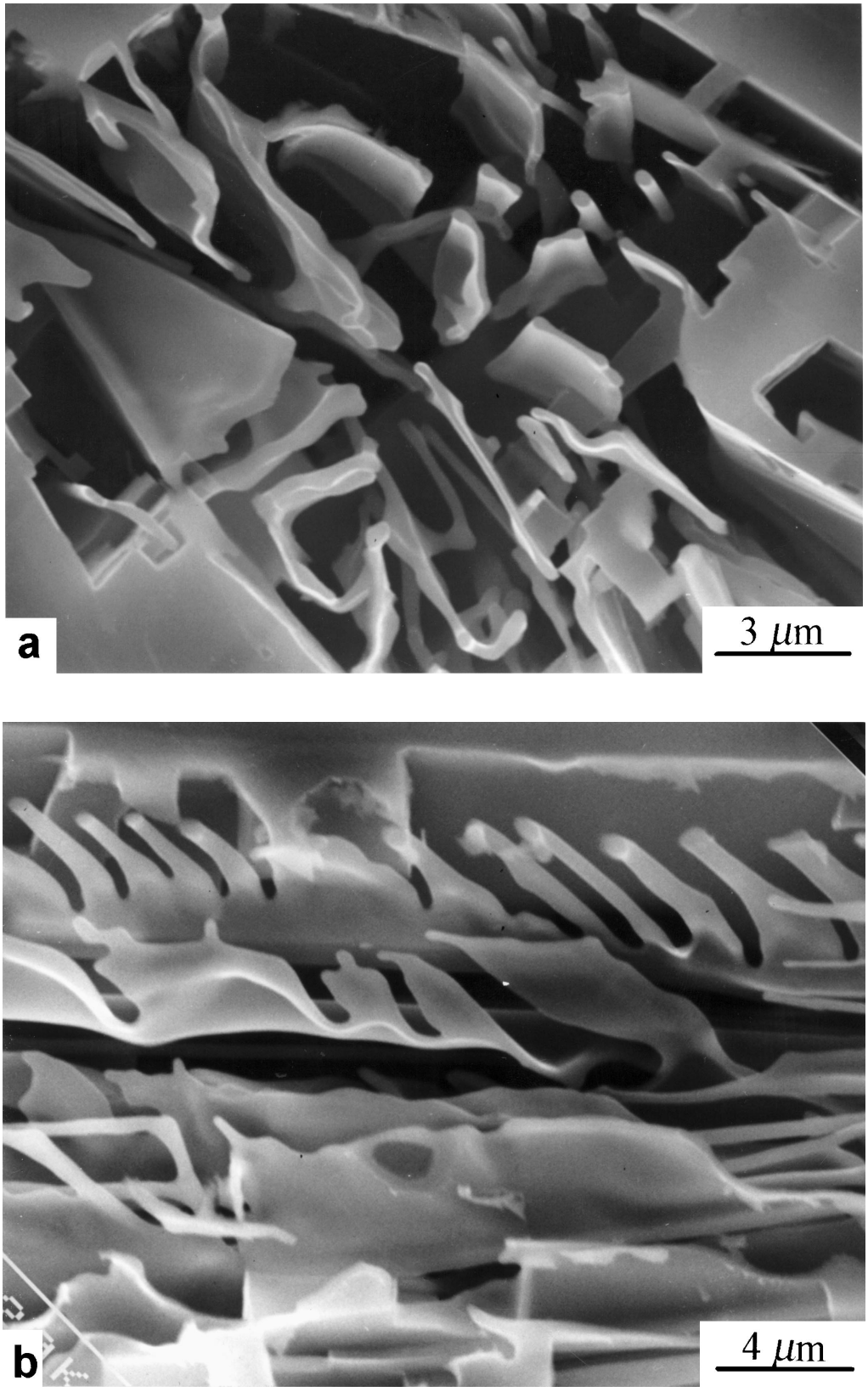

Figure 6 SEM micrographs showing the morphology of αAl-Al$_x$Fe eutectic in Al-2.85Fe-0.12V alloy grown at (a), (b) 200 μm/s, (c) and (d) 340 μm/s. (*Continued*).

became fibrous at high growth velocities. As shown in Figs 8a and b, the Al$_x$Fe rods in Eu3 were embedded in a continuous α-Al eutectic matrix at 810 and 1030 μm/s. The morphological transition from lamellar to rod-like with increasing growth velocity was observed to take place over the velocity range 200 to 510 μm/s and was complete at 810 μm/s. Compared with the cellular Eu2 structure observed in the binary Al-3Fe alloy from 200 to 1030 μm/s, cellular Eu3 structure was evident in the vanadium-containing alloy only at 810 and 1030 μm/s at which the morphological transition of Eu3 from lamellar to rod-like was complete.

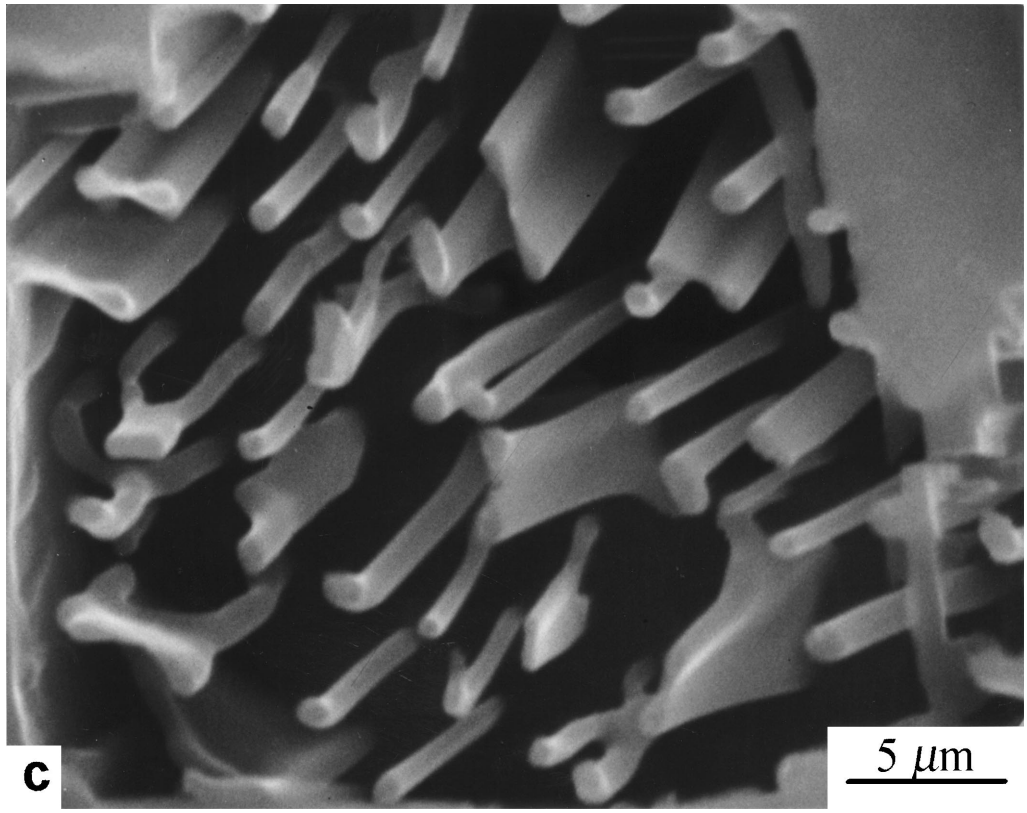

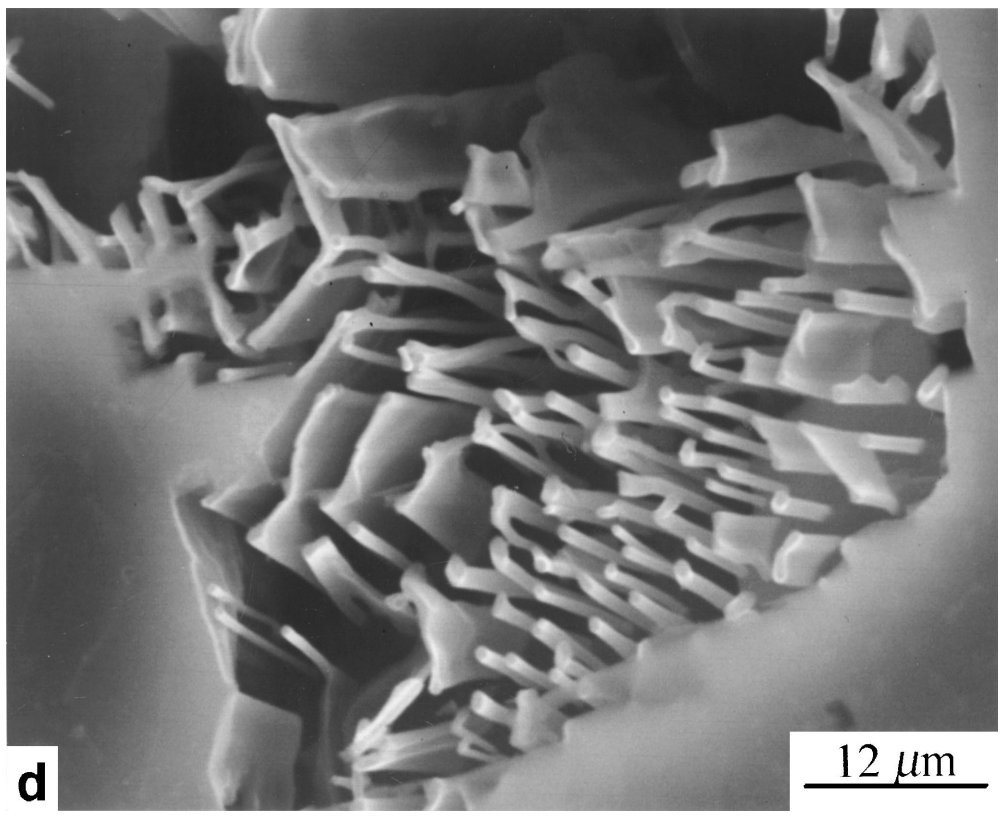

Figure 6 (*Continued*).

Figs 9a and b show the typical rod-like growth of Eu3 and a cell boundary where the Al_xFe rods tended to increase their diameter slightly. The rods were basically circular in cross-section with only small differences in diameter. There was no obvious evidence of crystallographic facetting of the Al_xFe eutectic intermetallic.

3.3. Solidification front configuration

Figs 10a and b are longitudinal section micrographs showing advancing solidification fronts quenched during steady state growth at a velocity of 100 μm/s for the two alloys. The solid/liquid (S/L) interface position prior to quenching was easily detected from the sudden

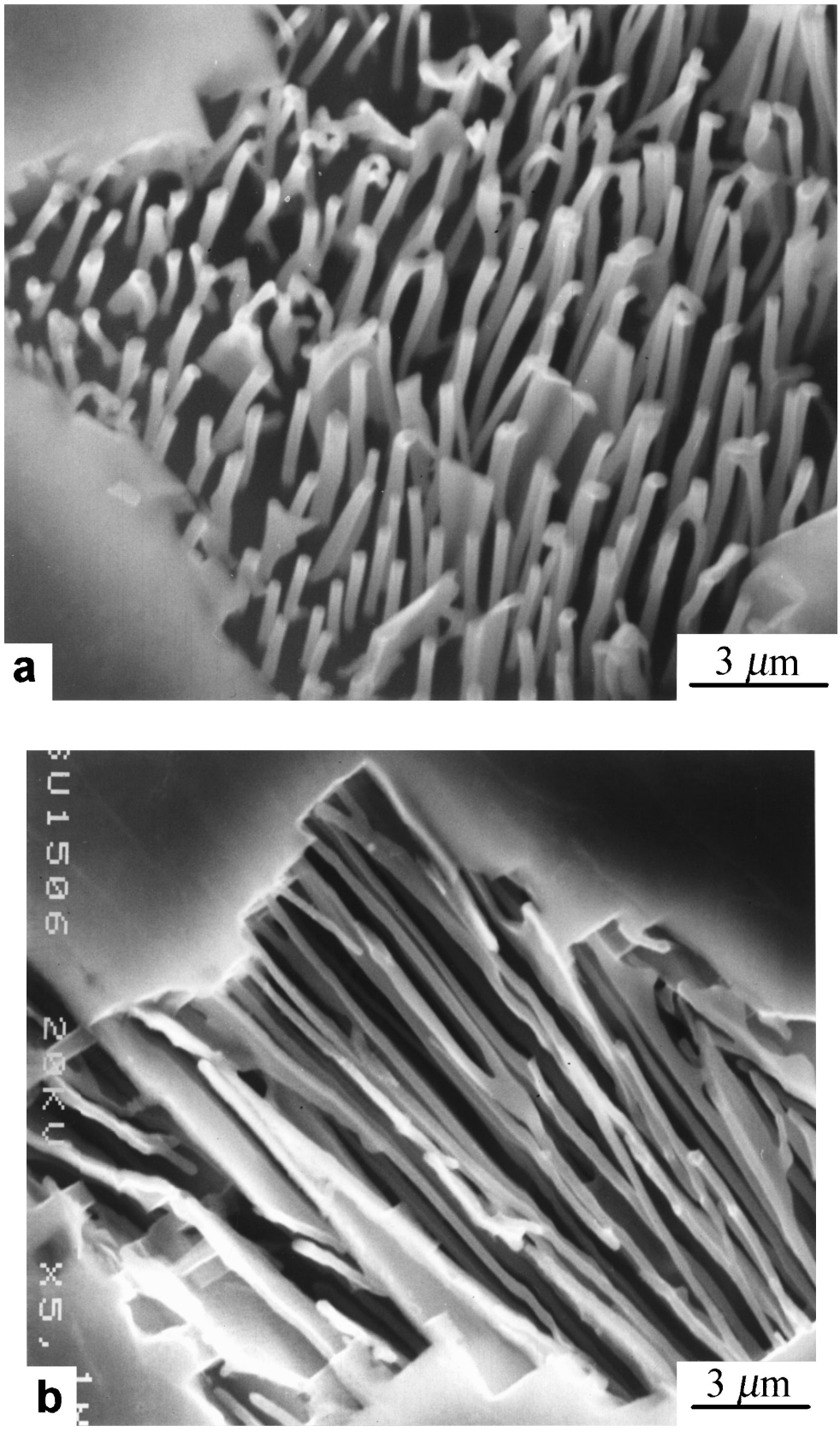

Figure 7 SEM micrographs showing the morphology of αAl-Al$_x$Fe eutectic in Al-2.85Fe-0.12V alloy grown at 510 μm/s (a) transverse and (b) longitudinal.

change in eutectic spacing in liquid solidified during the quench. The interface was essentially flat except for a few primary αAl dendrites protruding into the liquid ahead of the interface in the vanadium-containing alloy. The eutectic Al$_x$Fe lamellae were curved to deviate slightly from the overall growth direction. No evidence of significant protrusion from the interface of either eutectic Al$_6$Fe rods in Al-3Fe or Al$_x$Fe lamellae in Al-2.85Fe.0.12V was observed. A layer about 120 to 150 μm thick with fine eutectic structure was formed at

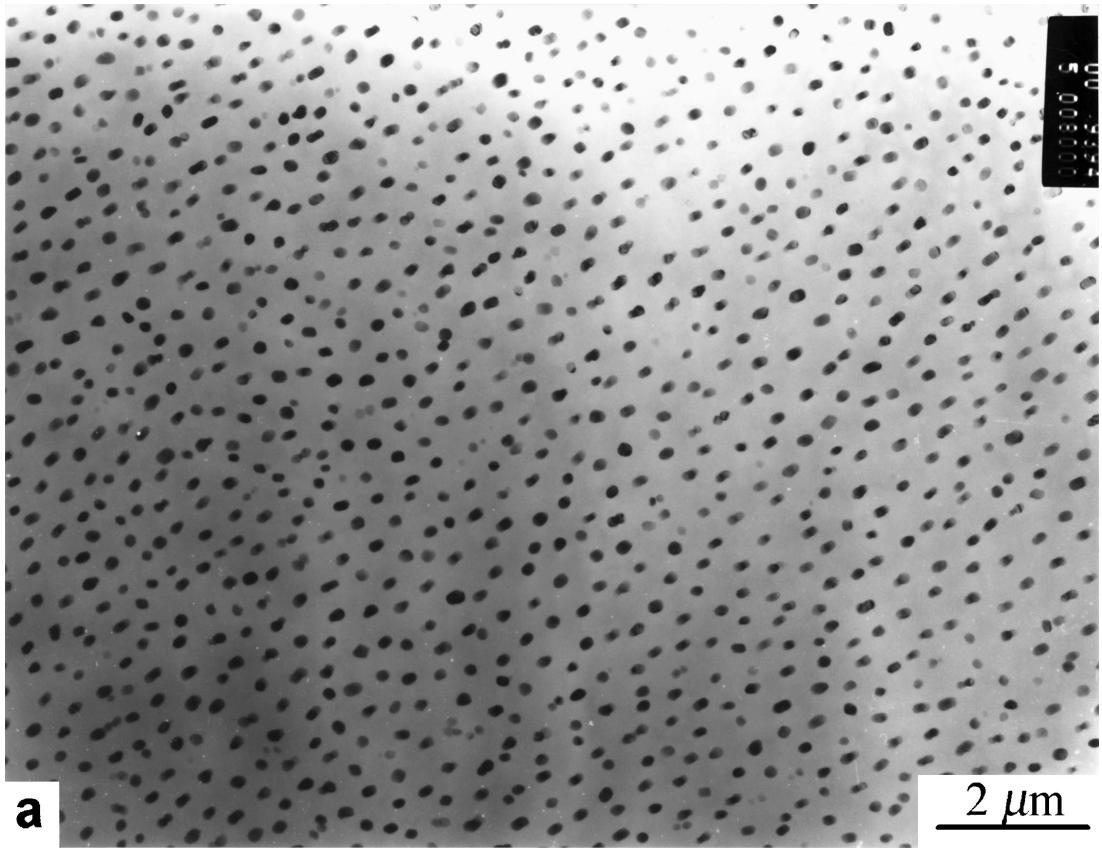

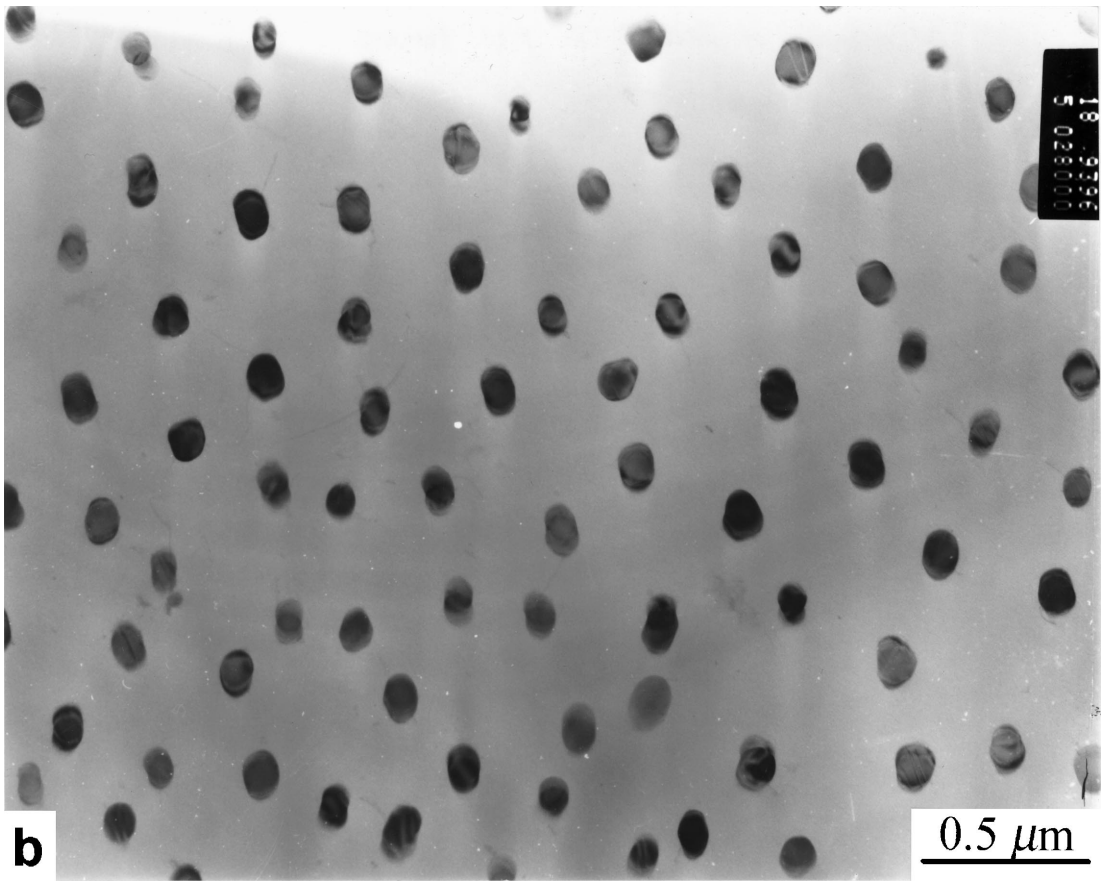

Figure 8 TEM micrographs showing rod-like αAl-Al_xFe eutectic in Al-2.85Fe-0.12V alloy grown at (a) 810 and (b) 1030 μm/s.

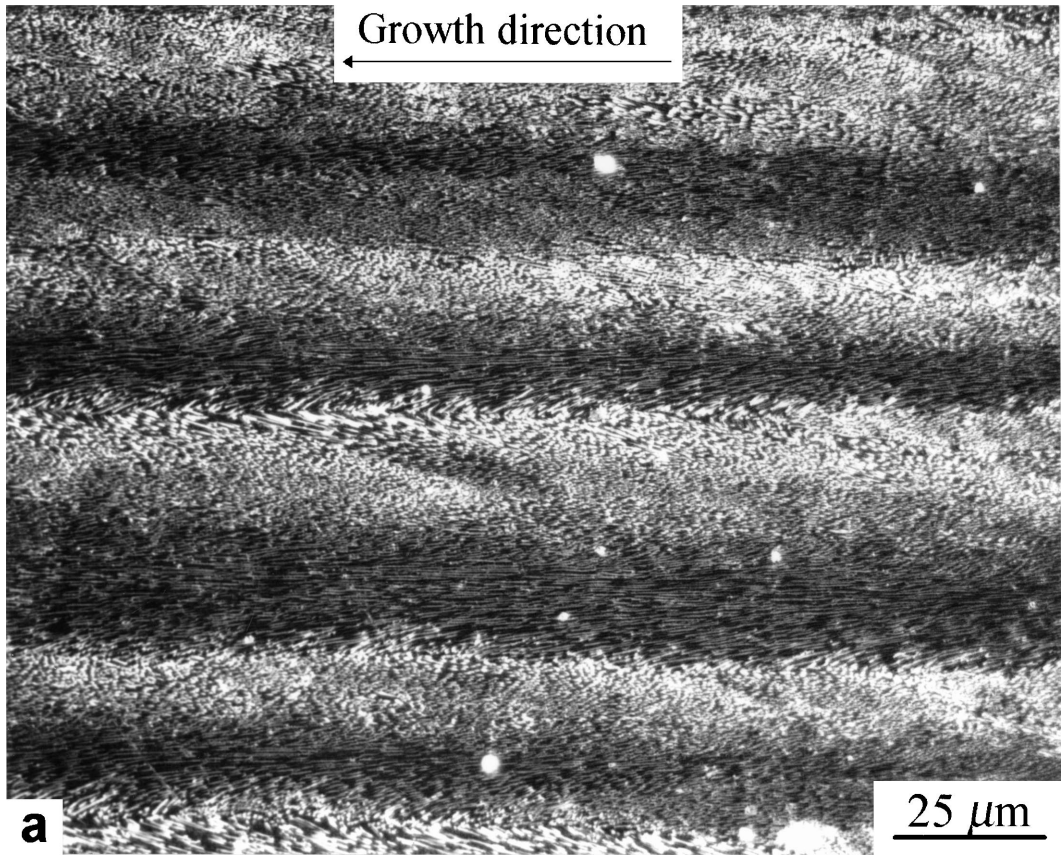

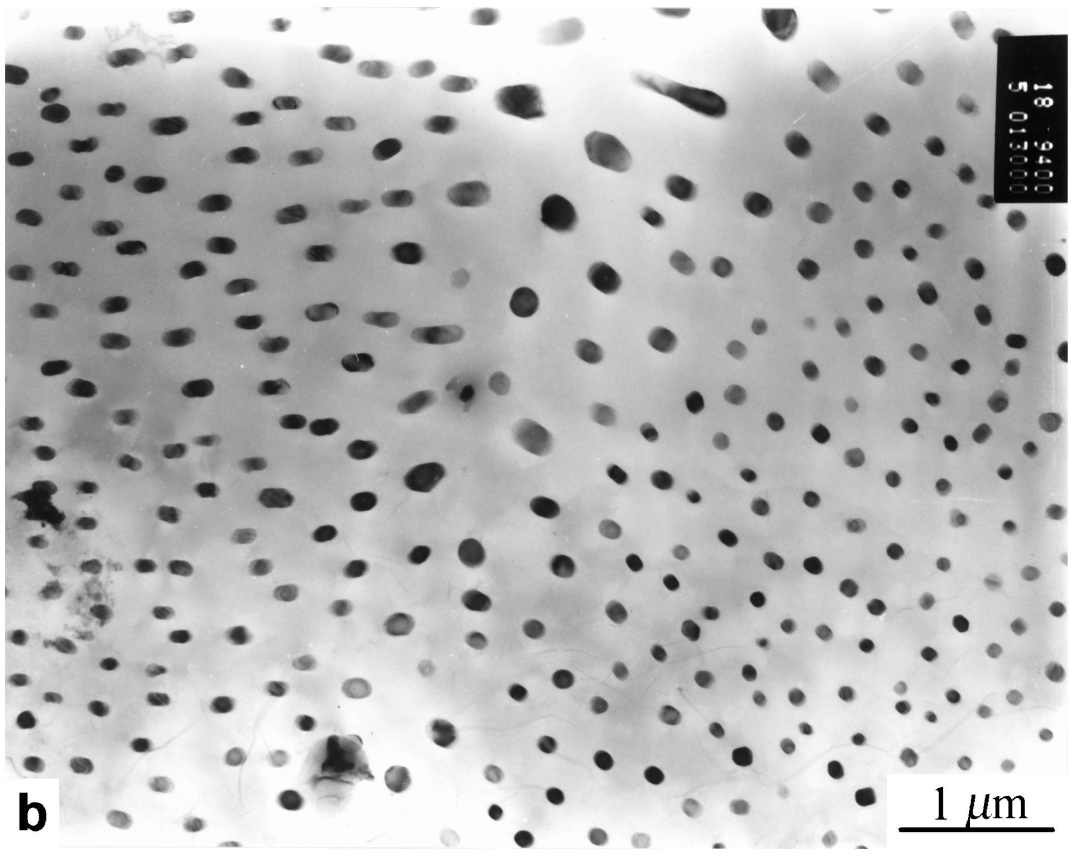

Figure 9 Optical and TEM micrographs showing (a) typical cellular growth of αAl-Al$_x$Fe eutectic and (b) a Eu3 cell boundary in Al-2.85Fe-0.12V alloy grown at 810 μm/s.

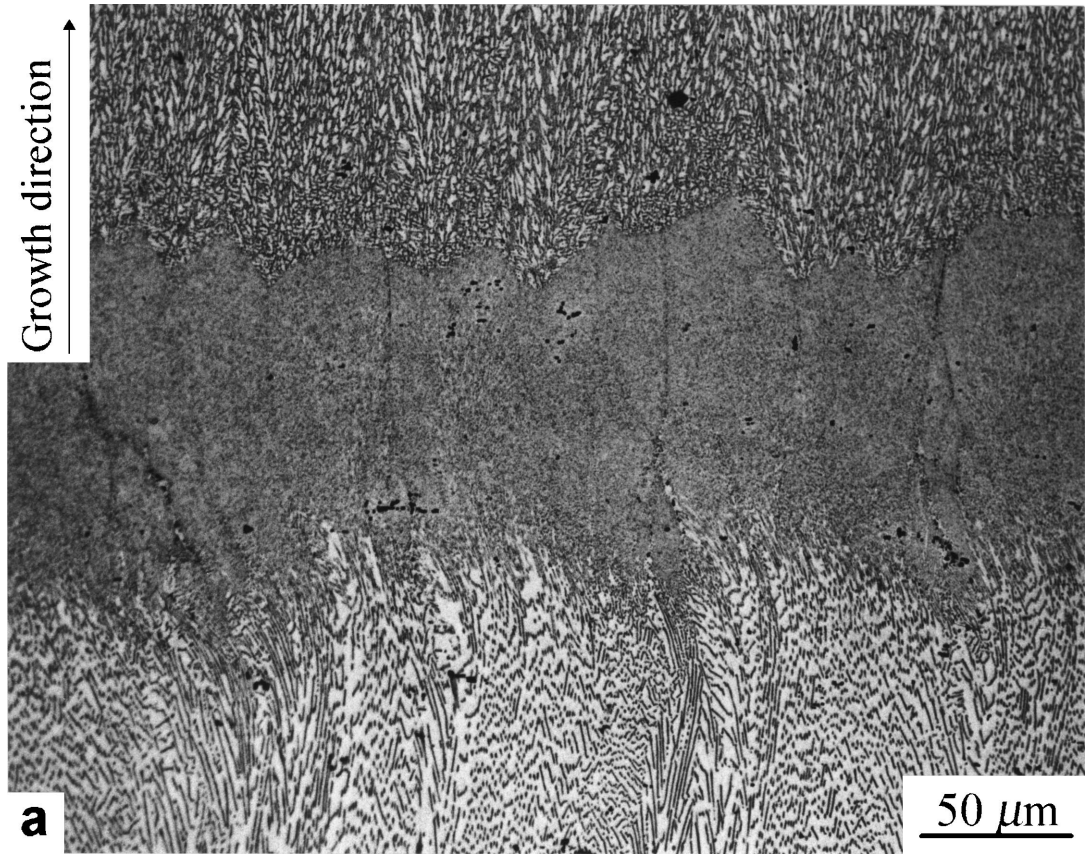

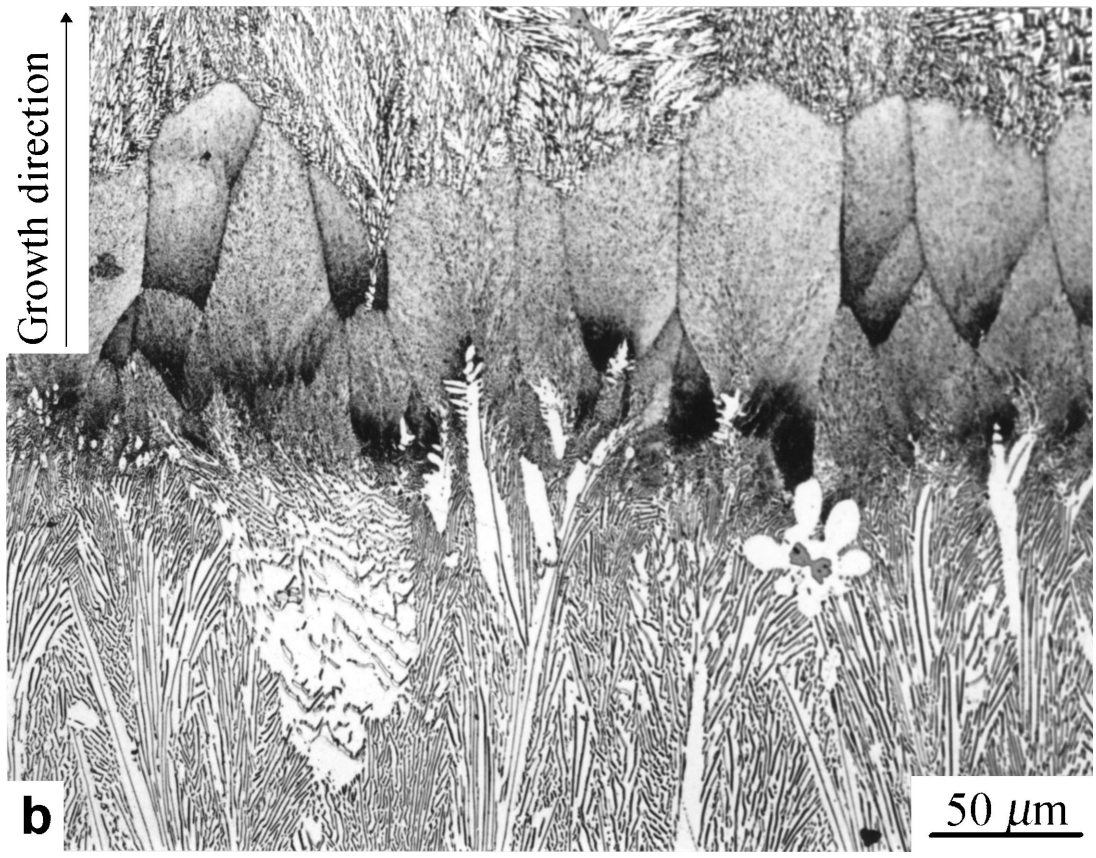

Figure 10 Optical micrographs showing the advancing solidification fronts quenched during steady state growth at 100 μm/s of (a) Al-3Fe and (b) Al-2.85Fe-0.12V alloys.

the interface for both alloys and αAl dendrites plus interdendritic eutectic structure was present beyond this layer. This layer exhibited a cellular structure similar to those obtained in high velocity steady state growth. At high growth velocity, a cellular eutectic structure was developed, as shown in Figs 9a and b. Al_xFe rods within the cells were parallel to each other but curved slightly towards the cell boundaries. From this observation an essentially flat S/L interface was indicated with small depressions only in the regions of the cell boundaries.

3.4. αAl-Al_xFe eutectic spacing

Direct measurement of mean eutectic spacing was performed on αAl-Al_xFe eutectic in the Al-2.85Fe-0.12V alloy by means of optical microscopy and TEM. For the samples in which lamellae and rods coexisted, such as those grown at 340 and 510 μm/s, the spacing measurement was carried out on both morphologies excluding the broken lamellae. It was noted that interlamellar spacing was larger than interrod spacing in the same samples with the two eutectic morphologies. Also, the regions adjacent to cell boundaries in the samples grown at 810 and 1030 μm/s were excluded from measurement. On plotting the mean inter-lamellar or inter-rod spacing λ, as a function of growth velocity v, as shown in Fig. 11, the relationship

$$\lambda = Av^{-1/2} \tag{1}$$

was found to apply with $A = 22.4 \pm 1.8$ and 13.8 ± 2.1 $\mu m^{3/2}\,s^{-1/2}$ for lamellar and rod-like eutectic morphologies, respectively.

4. Discussion

4.1. Effect of vanadium in displacing αAl-Al_6Fe by αAl-Al_xFe eutectic

For the binary Al-3Fe alloy the present study confirmed previously published results [1–3]. However, the solidification microstructure was significantly changed and Al_xFe intermetallic phase was stabilised as a eutectic constituent at growth velocity $v \geq 71$ μm/s when 0.12 wt % vanadium was added. Fully αAl-Al_xFe eutectic was obtained in the Al-2.85Fe-0.12V alloy over a wide range of growth velocity under the steady state growth conditions of the present study.

As a metastable intermetallic phase, Al_xFe was firstly reported as an interdendritic constituent in a hypoeutectic Al-Fe alloy by Young and Clyne [5] and then reported also by Westengen [6] and by Skjerpe [7]. Young and Clyne [5] suggested that Al_xFe could be an intermediate product in the eutectic transition between αAl-Al_3Fe and αAl-Al_6Fe. This is supported by the observation by Todd and Jones [11] of a transition from Al_xFe to Al_6Fe with increasing growth velocity for intercellular eutectic in Al-0.5 wt %Fe. However, when 0.1 wt %Si was added to the Al-0.5wt %Fe alloy, Al_xFe formed via Al_6Fe instead of via Al_3Fe with increasing growth velocity and even became dominant (some Al_3Fe was also present) at high velocities, such as 1000 and 2000 μm/s [11]. They suggested that the transition in dominant intermetallic phase to Al_xFe via Al_6Fe might be because of the reportedly low solid solubility of silicon in Al_6Fe, while Al_xFe could accommodate more silicon than Al_6Fe [14]. In our Al-2.85Fe-0.12V alloy, Al_3Fe was replaced by Al_xFe at 71 μm/s and higher velocities, but Al_6Fe was not detected even at the highest velocity, 1030 μm/s, in the present study. The mechanism by which vanadium promotes the formation of Al_xFe phase is not yet clear. The addition of vanadium, however, evidently favours formation of αAl-Al_xFe over αAl-Al_6Fe eutectic and extends to a lower growth velocity range the displacement of stable αAl-Al_3Fe by metastable αAl-Al_xFe.

Maggs [16] reported the effect of titanium (0.04 wt %) on the solidification microstructure of Bridgman grown Al-1.8 wt %Fe alloy. He found that titanium addition decreased the critical growth velocity for the transition from Eu1 to Eu3 and extended the growth velocity range over which Al_xFe can form, compared with the base binary Al-1.8 wt %Fe. The effect of titanium in stabilising Al_xFe was similar to that of vanadium found in the present study even though our alloy, Al-2.85Fe-0.12V, had a higher iron content. This similar effect of titanium and vanadium reflects the similar physical and chemical characteristics of these two alloying elements.

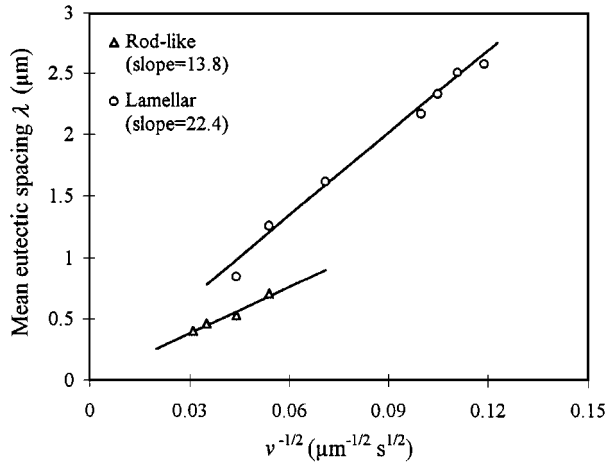

Figure 11 Dependence of mean αAl-Al_xFe eutectic spacing λ on growth velocity v.

4.2. Morphological transition of αAl-Al_xFe eutectic from lamellar to rod-like

Although morphological transition between lamellar (plate- or ribbon-like) and rod-like (fibrous) morphology has been reported previously for other eutectic systems e.g. [17–31], the change for αAl-Al_xFe eutectic from lamellar to rod-like with increasing growth velocity is reported here for the first time. The prevailing morphology of a unidirectionally solidified eutectic alloy is known to be generally dependent upon parameters such as temperature gradient G and growth velocity v, alloy composition and purity, and volume fraction ratio of the two eutectic components. The prediction based on minimum total interfacial free energy (for isotropic interfacial energy) [32] and minimum

growth undercooling [33] of preference for a fibrous over lamellar morphology for volume fractions of minor phase less than 0.28 [32] or 0.32 [33] is generally in accord with observations [34], with only a 25 percent anisotropic reduction in interfacial energy being required for the lamellar interface orientation to stabilise a lamellar structure down to volume fraction as low as 0.05 [33]. The observation of a lamellar morphology for the low volume fraction of Al_xFe in the αAl-Al_xFe eutectic is thus compatible with theory as well as with earlier observations for Al-Al_2Au [35], Al-Al_9Co_2 [36], Al-Al_4Ce [37], Al-Al_3Y [37] and Al-Al_4La [38]. Transition between lamellar and fibrous morphologies as a result of changes in composition [29], addition of impurities [18, 20, 22] or changes in growth velocity [24, 25, 30, 31] has been observed repeatedly. Thus lamellar morphology can be replaced by fibrous structures both at low [31, 32, 37, 39] and at high [20, 21, 25, 36, 37, 40–42] velocities. The high velocity transition from lamellae to fibres is explicable in terms of increased incidence of faulting in the lamellar structure. In the present system this is manifest, initially, as side branching of lamellae as shown in Fig. 6b, resulting in fibres linked by residual webs eventually being replaced by an array of frequently branched fibres. The tendency for lamellae to deviate increasingly from the growth direction towards the edge of eutectic cells resulting from impurities serves to enhance this destabilisation of lamellae at high growth velocity.

4.3. Dependence of eutectic spacing on growth velocity for the two morphologies

Both morphologies of the αAl-Al_xFe eutectic exhibited the predicted relationship [33] $\lambda\sqrt{v} = \text{constant } A$ (Equation 1) but with $A = 22 \pm 2\ \mu m^{3/2}\ s^{-1/2}$ for the lamellar morphology and $A = 14 \pm 2\ \mu m^{3/2}\ s^{-1/2}$ for the fibrous morphology. These values of A lie within the range 7 to 50 $\mu m^{3/2}\ s^{-1/2}$ found for αAl based eutectics [43]. For a volume fraction f of the minor phase, the Jackson-Hunt model predicts the ratio of $\lambda\sqrt{v}$ for a lamellar to a fibrous morphology as:

$$\frac{(\lambda\sqrt{v})_{lam}}{(\lambda\sqrt{v})_{rod}} = \frac{A_{lam}}{A_{rod}} = 2\left(\frac{M}{P}\right)^{1/2} f^{1/4} \qquad (2)$$

where M and P are tabulated functions of f. For $f \sim 0.1$, characteristic of αAl-Al_xFe eutectic, Equation 2 predicts $A_{lam}/A_{rod} = 2.8$ compared to our experimental value of 1.6. A more recent modification of the Jackson-Hunt model by Magnin and Trivedi [44] takes into account the effect on the diffusion field of density difference between the eutectic phase and replaces the isothermal interface coupling condition by an equilibrium condition for the three phase junction. This modified model predicts

$$\lambda_{lam}/\lambda_{rod} = 0.574/f^{0.415} \qquad (3)$$

which gives $\lambda_{lam}/\lambda_{rod} = 1.49$ much closer to our experimental value of 1.6.

5. Conclusions

1. Fully αAl-Al_xFe eutectic structure has been obtained in Al-2.85 wt %Fe-0.12V alloy by steady state growth over a velocity range from 71 to 1030 μm/s except at 100 and 510 μm/s where a few primary αAl dendrites were present in the eutectic matrix. This αAl-Al_xFe eutectic forms rather than the αAl-Al_6Fe eutectic observed in the binary Al-3 wt %Fe alloy for 91 to 1030 μm/s.

2. The αAl-Al_xFe eutectic underwent a morphological transition from lamellar to rod-like with increasing growth velocity and a cellular eutectic structure was developed when the eutectic was all rod-like.

3. The predicted relationship $\lambda = Av^{-1/2}$ between eutectic spacing λ and growth velocity v, was applicable with $A = 22.4 \pm 1.8$ and $13.8 \pm 2.1\ \mu m^{3/2}\ s^{-1/2}$ for lamellar and rod-like αAl-Al_xFe eutectic, respectively. The observed ratio $\lambda_{lam}/\lambda_{rod} = 1.6$ for fixed growth velocity v is close to the applicable value 1.5 predicted by the Magnin and Trivedi modification of the Jackson-Hunt model of eutectic growth.

Acknowledgements

One of the authors, Y. W., is grateful to the CVCP (ORS awards) and to Alcan International Ltd. for financial support for this work which formed part of a PhD program for him at Sheffield.

References

1. C. McL. ADAM and L. M. HOGAN, *J. Austral. Inst. Met.* **17** (1972) 81.
2. C. McL. ADAM, *idem, Acta Metall.* **23** (1975) 345.
3. I. R. HUGHES and H. JONES, *J. Mater. Sci.* **11** (1976) 1781.
4. H. KOSUGE and I. MIZUKAMI, *J. Jpn. Inst. Light Met.* **22** (1972) 437.
5. R. M. K. YOUNG and T. W. CLYNE, *Scripta Metall.* **15** (1981) 1211.
6. H. WESTENGEN, *Z. Metallkde* **73** (1982) 360.
7. P. SKJERPE, *Metall. Trans. A* **18A** (1987) 189.
8. P. LIU, T. THORVALDSON and G. L. DUNLOP, *Mater. Sci. Technol.* **2** (1986) 1009.
9. C. J. SIMENSEN and R. VELLASAMY, *Z.Metallkde* **68** (1977) 428.
10. P. G. KEONG, J. A. SAMES, C. McL. ADAM and R. M. SHARP, in "Solidification and Casting of Metals" (The Metals Society, London, 1979) p. 110.
11. I. TODD and H. JONES, *Mater. Sci. Forum* **217–222** (1996) 201.
12. L. BACKERUD, *Jernkont. Ann.* **152** (1968) 109.
13. L. R. MORRIS, in "Solidification and Casting of Metals" (The Metals Society, London, 1979) p. 218.
14. Y. LANGSRUD, *Key Eng. Mater.* **44/45** (1990) 95.
15. I. TODD, Ph.D. thesis, Sheffield, 1996.
16. S. J. MAGGS, Ph.D. thesis, Leeds, 1996.
17. J. D. HUNT and J. P. CHILTON, *J. Inst. Metals* **91** (1962/1963) 338.
18. M. G. DAY and A. HELLAWELL, *J. Austral. Inst. Met.* **9** (1964) 213.
19. J. D. HUNT, *J. Inst. Metals* **94** (1966) 125.
20. D. JAFFREY and G. A. CHADWICK, *ibid.* **97** (1969) 118.
21. D. JAFFREY *idem, Trans. Met. Soc. AIME* **245** (1969) 2435.
22. H. E. CLINE and J. L. WALTER, *Met. Trans.* **1** (1971) 2907.
23. H. E. CLINE, J. L. WALTER, E. LIFSHIN and R. R. RUSSELL, *ibid.* **2** (1971) 189.
24. W. KURZ and B. LUX, *ibid.* **2** (1971) 329.
25. H. B. SMARTT and T. H. COURTNEY, *ibid.* **3** (1972) 2000.
26. J. A. SPITTLE, *Metallography* **6** (1973) 115.

27. S. A. DAVID, A. T. SANTHANAM and H. D. BRODY, *Met. Trans. A* **7A** (1976) 1051.
28. S. A. SAVAS and R. W. SMITH, *J. Mater. Sci.* **20** (1985) 881.
29. N. B. SINGH, Z. KUN and T. HENNINGSEN, in "Solidification Processing 1987" (The Inst. of Metals, 1988) pp. 129–132.
30. M. A. ALAM NAJAFABADI, S. KHAN, A. OURDJINI and R. ELLIOTT, *Cast Metals* **8** (1995) 35.
31. M. YOSHIDA, T. TSUJIMURA, M. KAMATA and H. NAKAE, *J. Jpn. Inst. Metals* **59** (1995) 653.
32. D. J. S. COOKSEY, D. MUNSON, M. P. WILKINSON and A. HELLAWELL, *Phil. Mag.* **10** (1964) 745.
33. K. A. JACKSON and J. D. HUNT, *Trans. Met. Soc. AIME* **236** (1966) 1129.
34. L. M. HOGAN, R. W. KRAFT and F. D. LEMKEY, in "Advances in Materials Research," edited by H. Herman, Vol. 5 (New York 1971) pp. 83–125.
35. G. PIATTI and G. PELLEGRINI, *J. Mater. Sci.* **11** (1976) 913.
36. C. McL. ADAM and S. MARICH, *J. Austral. Inst. Met.* **17** (1972) 142.
37. K. N. STREET, C. F. ST. JOHN and G. PIATTI, *J. Inst. Metals* **95** (1967) 326.
38. H. DONG, Y. JI, J. ZHU, S. LU and X. ZHANG, *Acta Met. Sinica* **29** (1993), A102.
39. J. D. LIVINGSTON, *J Appl. Phys.* **41** (1970) 197.
40. R. RACEK, G. LESOULT and M. TURPIN, *J. Crystal Growth* **22** (1974) 210.
41. M. A. SAVAS, L. CLAPHAM and R. W. SMITH, *J. Mater. Sci.* **25** (1990) 909.
42. A. MOORE and R. ELLIOTT, *J. Inst. Metals* **96** (1968) 62.
43. J. A. JUAREZ-ISLAS and H. JONES, *Acta Met.* **35** (1987) 499.
44. P. MAGNIN and R. TRIVEDI, *Acta Met. Mater.* **39** (1991) 453.

Received 17 August
and accepted 18 September 1998